International Journal of Advanced Structural Engineering (2019) 11:255–270
https://doi.org/10.1007/s40091-019-0228-2

ORIGINAL RESEARCH

Confinement of six different concretes in CFST columns having different shapes and slenderness

Khandaker M. A. Hossain[1] · **Katie Chu**[1]

Received: 25 March 2018 / Accepted: 14 May 2019 / Published online: 18 May 2019

Abstract

This paper presents behaviour of normal concrete, ultrahigh-strength concrete, engineered cementitious composite, lightweight concrete, self-consolidating concrete and crumb rubber concrete under confinement. Forty-six circular, square and rectangular concrete-filled steel tube columns with varying slenderness are tested under axial compression. Failure modes, axial load–displacement responses and stress–strain characteristics are analysed as well as concrete confined strengths are determined based on experimental results and existing models. The performance of existing confined strength models is evaluated and modified to accommodate different types of high-performance concretes and column shapes. The modified model improves the prediction of confined concrete strength with a mean predicted-to-experimental ratio of 1.05 as shape and concrete type factors are introduced.

Keywords Concrete confinement · High-performance concrete · Composite columns · Concrete-filled steel tube · Confined concrete model

Introduction

Concrete-filled steel tube (CFST) columns have been a topic of research for the past 40 years (Shanmugam and Lakshmi 2001). Researchers noticed concrete strength enhancement and improved ductility of CFST columns (as shown in Fig. 1) due to confinement by the steel tube, which limits the extension of cracks and spalling (Ghosh 1977; Han et al. 2003; Fam et al. 2004; Yu et al. 2008; Khaloo et al. 2014). However, most of the research done in the past was based on circular columns infilled with normal concrete (NC). More recently, new generation of high-performance concretes (HPCs) have been developed by incorporating different materials (such as fibres, supplementary cementing materials, industrial wastes and lightweight aggregates) with superior fresh state, mechanical and durability properties than normal concrete. Ultrahigh-strength concrete (UHSC), engineered cementitious composite (ECC), lightweight concrete (LWC), self-consolidating concrete (SCC) and crumb rubber concrete (CRC) are several HPCs recently being developed, and their structural performance was evaluated by the Ryerson University research team (Sherir et al. 2018; Lotfy et al. 2016; Hossain et al. 2012a, b, 2018; Hassan et al. 2012; Mohammed et al. 2012).

UHSC has been studied as infill for steel tube columns before to find that higher-strength concrete resulted in decreased ductility (Yu et al. 2008). However, UHSC used in the past research typically included coarse aggregates without steel fibre reinforcements. Steel fibre reinforcements have been found to improve concrete ductility (Khaloo et al. 2014), and such type of fibre-reinforced UHSC is expected to improve strength and ductility of CFST columns.

The fresh state, mechanical and durability properties of ECCs are the subject matters of intense research over the recent years (Sherir et al. 2018; Özbay et al. 2013). ECC typically incorporates cementitious materials (such as fly ash or slag) along with fine aggregates such as silica sand or crushed sand, and fibre (typically polyvinyl alcohol fibre) reinforcement. ECC has shown to provide several advantages over NC. For example, the strain hardening capacity of ECC was found to be 300–500 times that of NC (Weimann and Li 2003). The superior strain hardening, multiple microcracking and ductility characteristics of ECC are expected to improve confinement in CFST columns.

✉ Khandaker M. A. Hossain
ahossain@ryerson.ca

[1] Department of Civil Engineering, Ryerson University, 350 Victoria Street, Toronto, ON M5B 2K3, Canada

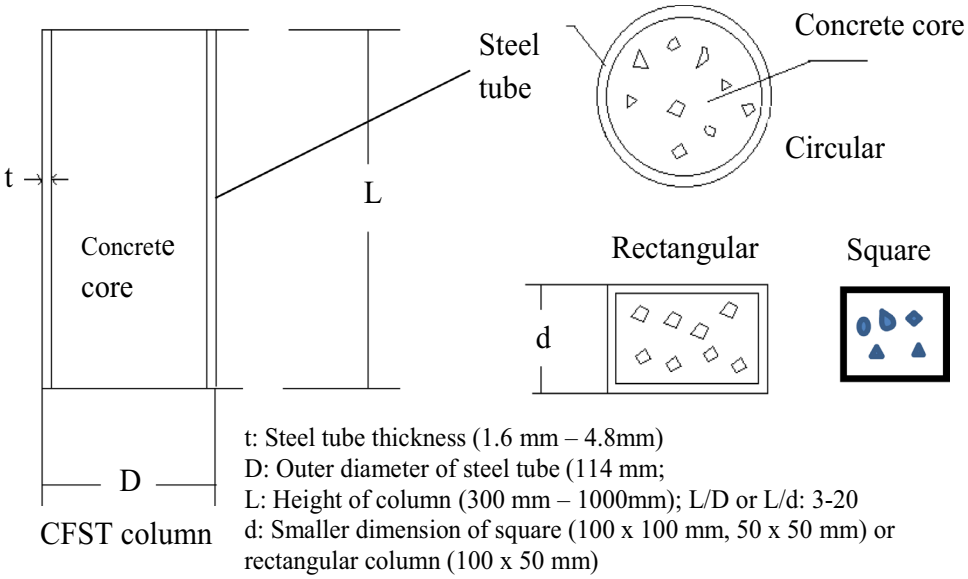

Fig. 1 CFST columns with circular, rectangular and square cross section

LWCs made with natural or artificial lightweight aggregates are useful for reducing deadweight of structures (Hossain 2004). Hossain (2003) experimented lightweight volcanic pumice concrete in steel hollow sections to find that the strength was comparable with those columns infilled with NC. More research is needed to explore the behaviour of LWCs with various lightweight aggregates (such as pumice, slag, expanded shale and expanded clay) as infill in CFST columns to quantify the effect of steel tube confinement.

Crumbed rubber tires have been incorporated into concrete to form CRC (Mohammed et al. 2012). Crumb rubber has improved NC ductility and energy absorption. However, no literature has been found on the use of CRC in composite structures. CRC typically has lower compressive strength compared with NC. But strength of CRC can be enhanced by confinement by the steel tube columns. Therefore, steel tube columns with CRC infill are expected to improve ductility and strength.

The behaviour of normal weight SCC-filled steel tube columns has been investigated in the past (Han et al. 2005; Lachemi et al. 2006a, b). SCC speeds construction processes by eliminating the need for external compaction during casting. This also reduces noise and labour involved with concrete casting. In most cases, behaviour of columns infilled with SCC was similar to that of their NC-filled counterparts. Recent research at Ryerson University has developed SCCs with lightweight aggregates (such as slag, pumice, expanded shale and expanded clay) (Lotfy et al. 2016). However, not much literature is available for quantifying the behaviour of SCC and lightweight SCC under steel tube confinement.

This research provides new insights especially into the contribution of several HPCs to axial strength of CFST columns. This research is very significant and relevant considering the lack of research studies on quantifying the confining strength of new generation HPCs in CFSTs and on performance of existing models (developed for normal concrete) to predict HPC confined strength. Existing models for quantification of concrete strength under confinement are available in the literature (Richart et al. 1928; Mander et al. 1988; O'Shea and Bridge 2000). This paper presents the behaviour of NC and new generation of self-consolidating HPCs (such as UHSC, ECC, LWC, SCC and CRC) under steel tube confinement based on comprehensive experimental and theoretical investigations on CFST columns. The variables in CFSTs used in this research are: shape (circular, square and rectangular), slenderness ratio (height to diameter or height to minimum cross-sectional dimension), steel tube thickness and infill concrete types (six types—normal weight or lightweight, self-consolidating or not consolidating, with/without coarse aggregate and with or without fibre). The behaviour CFSTs with various HPCs subjected to monotonic concentric axial loading to failure is described and compared based on load–deformation/strain responses, steel tube buckling and failure modes. In addition, the performance of existing models in predicting confined concrete strength is evaluated and a modified confinement model is proposed based on results of current and previous research studies. The findings and recommendations of this research will surely benefit engineers and researchers to understand the behaviour of CFSTs with various HPCs through quantifying their confined compressive strength using existing and proposed models.

Experimental programme

A total of 46 CFST columns were tested as summarized in Table 1. The experiments were carried out to determine strength of concrete confined by steel tubes by collecting axial and hoop strain data and axial load–displacement response of columns under axial concentric loading. The variables in the tests were selected to better understand the effects of CFST columns cross-sectional shape, concrete type and slenderness (length-to-diameter ratio) on confinement strength of different types of concretes.

Geometric descriptions

CFST columns were made of commercially manufactured steel hollow structural tube sections having different thickness (t) infilled with six types of concretes. Schematic diagram of a CFST column showing different cross-sectional dimensions are shown in Fig. 1. Four different column shapes were used for experimentation, including circular ('cI') shown in Table 1a, rectangular ('*r*') shown in Table 1b and two sizes of square ('s4' for 100 mm × 100 mm dimensions and 's2' for 50 mm × 50 mm dimensions) shown in Table 1c. The column slenderness ratio is defined as the length-to-diameter (*L*/*D*) ratio for circular columns and length-to-depth (*L*/*d*) ratio for square or rectangular columns with d as the smaller dimension of rectangular cross section (Fig. 1). Each steel hollow section was filled with one of the six concretes, namely normal concrete (NC), engineered cementitious composite (ECC), lightweight concrete (LWC), ultrahigh-strength concrete (UHSC), ordinary self-consolidating concrete (SCC) and crumb rubber concrete (CRC).

100 mm × 200 mm cylinder compressive strength (f'_c) of all concretes at the age of testing and yield strengths (f_y) of steel tube obtained from a minimum of three coupon tests are provided in Table 1. The first letter in the column designation (Table 1) represents concrete type (N for NC, E for ECC, L for LWC, U for UHSC, S for SCC and R for CRC), second letter represents shape (cI for circular, r for rectangular and S4 or S2 for square), and numeric represents slenderness ratio.

Casting, curing, instrumentation and testing of CFSTs

NC was made with commercially available pre-packaged dry contents, to which 2.4 L of water was added during mixing for every 30-kg bag. Dry contents included nominal aggregate size of 10 mm, Portland cement, silica fume and air-entraining admixture. UHSC was made of Type 10 cement, silica sand, undensified silica fume, high-range water-reducing admixture and 13-mm-long straight steel fibres with diameter of 0.2 mm. ECC used in this research is comprised of Type 10 Portland cement with 55% class F fly ash replacement, silica sand, polyvinyl alcohol fibres and high-range water-reducing admixture. Commercially available coarse and fine pelletized slag aggregate was used for producing LWC in addition to slag aggregates, Type 10 Portland cement, class F fly ash, densified silica fume and high-range water-reducing admixture. CRC was produced by incorporating Type 10 Portland cement, slag, 19-mm maximum size coarse aggregate, natural sand, crumbed rubber of 600 μm size as 20% sand replacement by volume and high-range water-reducing admixture.

All concretes were self-consolidating except NC. Self-consolidating concretes compact under their own weight without additional vibration or tamping. Specimens were casted in a vertically upright position, and self-consolidating concretes (ECC, LWC, UHSC, SCC and CRC) were poured from the top and cast without applying physical compaction. NC was placed in layers and compacted on a vibrating table. The steel tube was used as formwork, and the bottom of the tube was sealed at the base to prevent leakage and loss of materials during casting. Control concrete specimens in the form of 100 × 200 mm cylinders were cast and tested alongside CFST columns to determine compressive strength. All specimens were air-cured until testing.

CFST column ends were ground flat to ensure that the load was applied evenly over the entire cross section. Strain gauges were attached at the mid-height of columns (Fig. 2). One gauge was oriented in the vertical direction for measuring axial strain, while the other was oriented along the horizontal direction for measuring transverse strain. Columns were placed vertically in a hydraulic compression machine, and load was applied monotonically at a rate of 0.2 MPa/s (as shown in Fig. 2) until failure. Axial load–displacement/strain responses were recorded through a computer-aided data acquisition system during the loading history, while overall behaviour of columns such as steel tube buckling and failure modes was also obser*v*ed visually.

Analysis of results and discussion

Load–displacement response and failure modes

Table 2 summarizes the failure modes and axial strengths of CFST columns subjected to monotonic concentric compression loading. Typical failure modes of CFST columns (such as radial expansion, local buckling, plastic hinge, shear and global buckling) are shown in Fig. 3. CFST columns with slenderness ratio of 3 (circular or square) failed by radial expansion in most cases.

Table 1 Column specifications

(a) Circular columns

CFST designation	Concrete type	Concrete strength (MPa)	Steel tube yield strength (f_y) (MPa)	Diameter (D) (mm)	Steel tube thickness (t) (mm)	Length (L) (mm)
NcI-3	NC	66	333	114	4.8	300
EcI-3	ECC	50	333	114	4.8	300
LcI-3	LWC	36	333	114	4.8	300
UcI-3	UHSC	127	333	114	4.8	300
ScI-3	SCC	56	333	114	4.8	300
RcI-3	CRC	46	333	114	4.8	300
NcI-9	NC	66	333	114	4.8	1000
EcI-9	ECC	50	333	114	4.8	1000
LcI-9	LWC	66	333	114	4.8	1000
UcI-9	UHSC	127	333	114	4.8	1000
ScI-9	SCC	56	333	114	4.8	1000
RcI-9	CRC	46	333	114	4.8	1000

(b) Rectangular columns

CFST designation	Concrete type	Concrete strength (f'_c) (MPa)	Steel tube yield strength (f_y) (MPa)	Breadth (b) (mm)	Depth (d) (mm)	Steel tube thickness (mm)	Length (L) (mm)
Nr-6	NC	66	372	100	50	3.2	300
Er-6	ECC	50	372	100	50	3.2	300
Lr-6	LWC	36	372	100	50	3.2	300
Ur-6	UHSC	127	372	100	50	3.2	300
Sr-6	SCC	56	372	100	50	3.2	300
Rr-6	CRC	46	372	100	50	3.2	300
Nr-20	NC	66	372	100	50	3.2	1000
Er-20	ECC	50	372	100	50	3.2	1000
Lr-20	LWC	36	372	100	50	3.2	1000
Ur-20	UHSC	127	372	100	50	3.2	1000
Sr-20	SCC	56	372	100	50	3.2	1000
Rr-20	CRC	46	372	100	50	3.2	1000

(c) Square columns

CFST designation	Concrete type	Concrete strength (f'_c) (MPa)	Steel tube yield strength (f_y) (MPa)	Breadth (b) (mm)	Depth (d) (mm)	Steel tube thickness (mm)	Length (L) (mm)
Ns4-3	NC	66	351	100	100	3.2	300
Es4-3	ECC	50	351	100	100	3.2	300
Ls4-3	LWC	36	351	100	100	3.2	300
Us4-3	UHSC	127	351	100	100	3.2	300
Ss4-3	SCC	56	351	100	100	3.2	300
Ns4-10	NC	66	351	100	100	3.2	1000
Es4-10	ECC	50	351	100	100	3.2	1000
Ls4-10	LWC	36	351	100	100	3.2	1000
Us4-10	UHSC	127	351	100	100	3.2	1000
Ss4-10	SCC	56	351	100	100	3.2	1000
Ns2-6	NC	66	365	50	50	1.6	300
Es2-6	ECC	50	365	50	50	1.6	300
Ls2-6	LWC	36	365	50	50	1.6	300
Us2-6	UHSC	127	365	50	50	1.6	300

Table 1 (continued)

(c) Square columns

CFST designation	Concrete type	Concrete strength (f'_c) (MPa)	Steel tube yield strength (f_y) (MPa)	Breadth (b) (mm)	Depth (d) (mm)	Steel tube thickness (mm)	Length (L) (mm)
Ss2-6	SCC	56	365	50	50	1.6	300
Rs2-6	CRC	46	365	50	50	1.6	300
Ns2-20	NC	66	365	50	50	1.6	1000
Es2-20	ECC	50	365	50	50	1.6	1000
Ls2-20	LWC	36	365	50	50	1.6	1000
Us2-20	UHSC	127	365	50	50	1.6	1000
Ss2-20	SCC	56	365	50	50	1.6	1000
Rs2-20	CRC	46	365	50	50	1.6	800

Fig. 2 Test set-up with instrumentation

Table 2 Failure mode and axial strength of CFSTs

Column designation		Failure mode		Axial strength (kN)	
(a)	(b)	(a)	(b)	(a)	(b)
NcI-3	NcI-9	Radial expansion	Shear	1410	1511
EcI-3	EcI-9	Radial expansion	Global buckling	1027	1113
LcI-3	LcI-9	Radial expansion	Global buckling	1148	982
UcI-3	UcI-9	Radial expansion	Shear	1681	1573
ScI-3	ScI-9	Radial expansion	Global buckling	1229	1111
RcI-3	RcI-9	Local buckling	Global buckling	1146	1046
Nr-6	Nr-20	Radial expansion	Shear	716	639
Er-6	Er-20	Local buckling	Shear	480	539
Lr-6	Lr-20	Local buckling	Global buckling	518	489
Ur-6	Ur-20	Shear	Global buckling	809	754
Sr-6	Sr-20	Local buckling	Shear	649	631
Rr-6	Rr-20	Shear	Global buckling	522	558
Ns4-3	Ns4-10	Radial expansion	Local buckling	1217	1204
Es4-3	Es4-10	Radial expansion	Local buckling	941	886
Ls4-3	Ls4-10	Local buckling	Local buckling	889	812
Us4-3	Us4-10	Radial expansion	Local buckling	1535	1446
Ss4-3	Ss4-10	Radial expansion	Plastic hinge	1013	768
Ns2-6	Ns2-20	Shear	Shear	266	309
Es2-6	Es2-20	Local buckling	Global buckling	176	184
Ls2-6	Ls2-20	Local buckling	Plastic hinge	187	167
Us2-6	Us2-20	Shear	Global buckling	330	326
Ss2-6	Ss2-20	Plastic hinge	Global buckling	202	225
Rs2-6	Rs2-16	Local buckling	Shear	168	168

In general, CFST columns with slenderness from 9 to 20 often failed by global buckling or shear. Columns with slenderness ratio of 6 (square or rectangular) failed by local buckling or shear in most cases. However, the 100 mm dimension square columns with slenderness of 10 mostly failed by local buckling. Shear failure occurred most often in columns filled with NC and UHSC, and these concretes had relatively higher compressive strength. In contrast, none of the CFSTs infilled with LWC (which had the lowest compressive strength compared with other concretes) failed in shear.

Axial strength of CFST columns depends on cross-sectional shape, steel tube thickness, concrete infill type, slenderness ratio and failure modes. Figure 4 illustrates the effect of cross-sectional shape and concrete type on axial load–displacement responses of CFST columns. CFSTs

(a) Radial expansion **(b)** Local buckling **(c)** Plastic hinge **(d)** Shear **(e)** Global buckling

Fig. 3 Classification of CFST column failure modes

with NC were taken as an example in Fig. 4a to compare axial load–displacement responses of 'cI' (circular), 's4' (square), 's2' (square) and 'r' (rectangular) sections. It can be observed that prior to the first peak load, all columns exhibited an increase in load at relatively same constant rate. CFSTs with higher slenderness exhibited lower first peak load. Rectangular and square sections exhibited similar responses after the first peak load with post-peak axial load decreased more significantly compared with the circular section. In addition, rectangular and square columns showed multiple peaks, while the circular column only experienced one peak load. Large post-first peak displacement of all CFST columns showed large ductility behaviour of such system.

Axial load–displacement responses of CFSTs with different types of concrete infill are shown in Fig. 4b. Axial load–displacement responses of CFSTs (NcI-3, UcI-3 and ScI-3) infilled with higher-strength concretes (NC, UHSC and SCC, respectively) showed slightly higher decrease in load after the first peak. On the other hand, CFSTs infilled with weaker concretes (ECC, CRC and LWC) did not show any obvious decrease in load when entering from elastic to plastic stages.

In general, an increase in axial strength (less than 10% in most cases) with the increase in slenderness was observed with exceptions of some columns (Table 2). Increase in axial strength of 14.5%, 6.4%, 9.6% and 8.7% for circular LWC, UHSC, SCC and CRC columns, respectively, was observed when slenderness ratio increased from 3 to 9. On the other hand, 1.1%, 5.8%, 8.7%, 5.8% and 24.2% increase in axial strength was observed for NC, ECC, LWC, UHSC and SCC square S4 columns, respectively, when slenderness ratio increased from 3 to 10.

Comparing the ratio (N/N_{NC}) of axial strength of column (N) to that of NC column (N_{NC}), axial capacity of UHSC-filled columns (ratio ranges between 1.13 and 1.26) was the highest, followed by NC (ratio 1.0), SCC (0.76 and 0.91), LWC (0.70 and 0.81), ECC (0.66 and 0.77) and CRC (0.63 and 0.81) for slenderness ranging from 3 to 6. For slenderness ranging from 9 to 20, ratio varied from 1.04 to 1.20 for UHSC, 1.0 for NC, 0.64 to 0.99 for SCC, 0.64 to 0.84 for ECC, 0.54 to 0.87 for CRC and 0.54 to 0.77 for LWC. The highest axial strength was observed in 'cI' sections (circular), followed by 's4' (square), 'r' (rectangular) and 's2' (square) columns when comparing steel tubes infilled with the same concrete type.

Strain characteristics

Figure 5 compares axial and transverse strain characteristics of selected CFST columns. A comparison of strain development in CFSTs with different shapes and slenderness ratio infilled with NC is presented in Fig. 5a. The 'cI' (circular) and 's4' (square) shapes had higher cross-sectional area and developed higher axial and transverse strain compared to 's2' shapes with smallest sectional area. The axial and

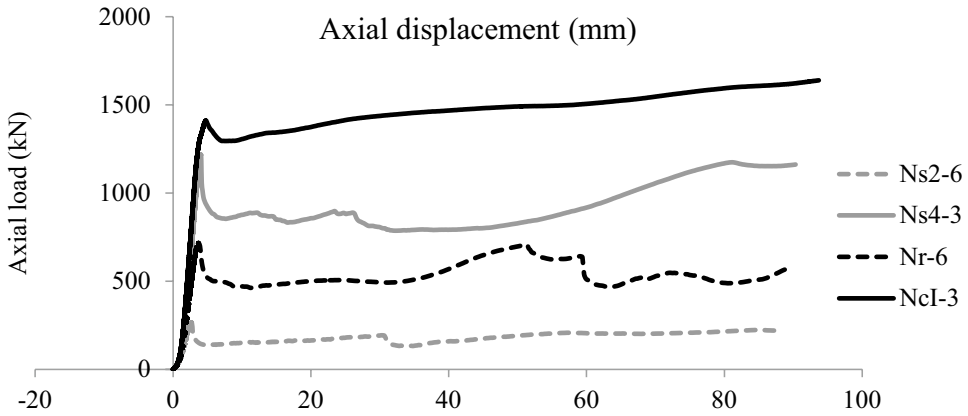

(a) Axial load-displacement response of CFST with various sectional shapes

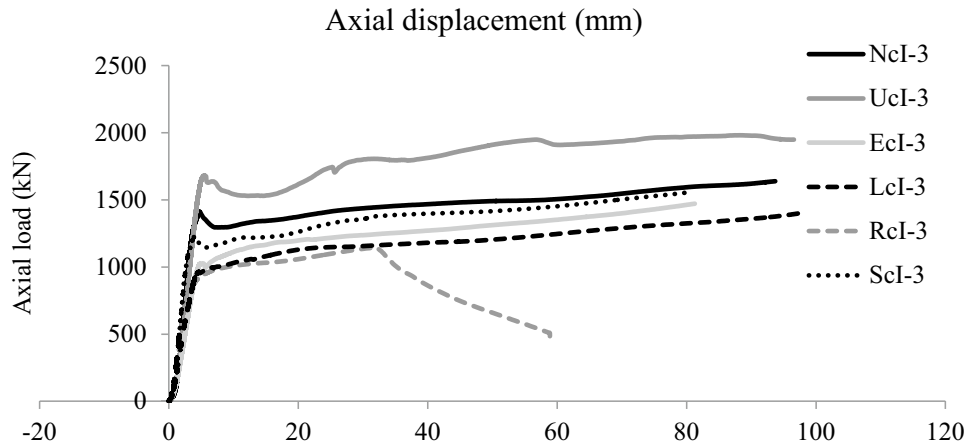

(b) Axial load-displacement response of CFST with various concrete types

Fig. 4 Axial load–displacement response of CFST columns

transverse strains in CFST columns with lower slenderness ratio of 3.0 reached yield strain.

Figure 5b shows strain development in circular CFSTs (having same slenderness ratio of 3.0) with different concrete infill. Strain development in CFST columns was found to be dependent on concrete type and their properties (strength and deformation characteristics). Steel strain in NcI-3, UcI-3 and ScI-3 columns having comparatively high-strength concrete (NC, UHSC and SCC, respectively) did not increase significantly during early stages of loading with UHSC-infilled UcI-3 showing lowest strain, especially in the axial direction due to less axial load carried by steel tube. Columns infilled with comparatively lower-strength concretes (such as ECC, LWC and CRC) developed higher steel strain at earlier stages of loading compared with NC, UHSC and SCC. Axial and transverse strains reached the yield strain of steel tube.

Table 3 provides axial strain at ultimate axial load of CFST columns, showing that developed strain exceeded yield strain of steel tube in almost all columns. Furthermore in most cases, lower axial strain was developed in columns with higher slenderness compared to their shorter counterparts. As previously mentioned, axial strain was higher for columns with larger cross-sectional area and steel thickness. Axial strain at ultimate load for columns with different infill can be compared. For example, circular LcI-6 column had axial strain of 0.0143, which was higher than other columns of the same shape infilled with different concretes. Columns infilled with LWC and ECC tended to show greater axial strain at ultimate load compared to their NC counterparts. This might be attributed to the higher load transfer to the steel tube in LWC/ECC column to offset higher deformation in weak concrete core for composite action.

Figure 6 shows the von Mises failure envelope defined by Eq. (1) obtained by plotting experimental axial and transverse stresses (Lachemi et al. 2006a):

$$f_{ys}^2 = \sigma_a^2 + \sigma_h^2 - \sigma_a \sigma_h, \quad (1)$$

Fig. 5 Strain characteristics of CFST columns

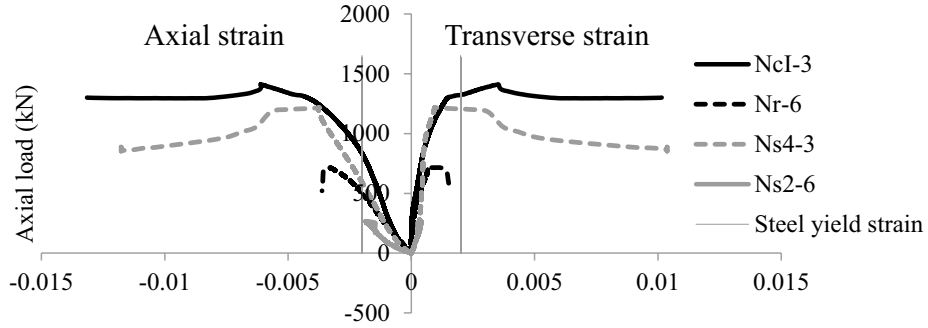

(a) Comparison of strain characteristics for CFSTs with different shapes

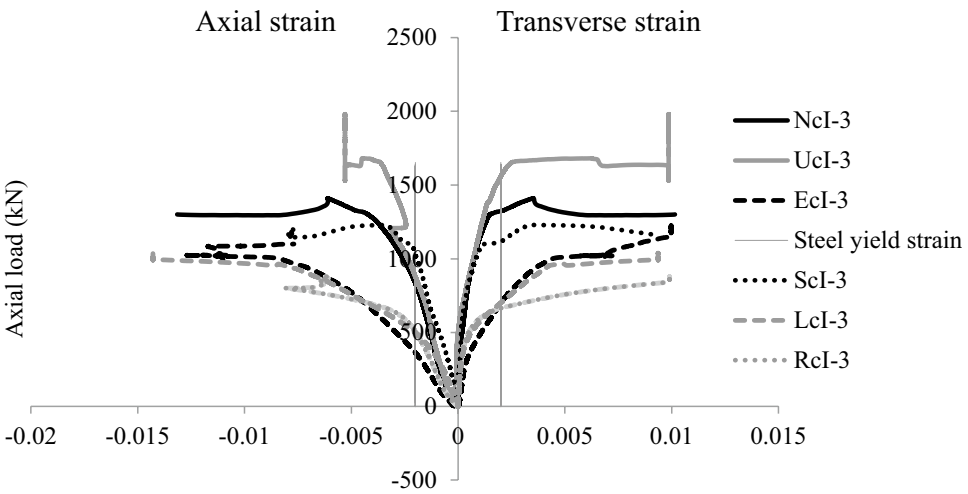

(b) Comparison of strain characteristics for CFSTs with different concrete in-fill

where von Mises yield strength (f_{ys}) is taken as the uniaxial steel yield strength (f_y) in Eq. (1), σ_a and σ_h are axial and hoop stresses, respectively, determined from experimental strains.

Figure 6 also shows the determination of axial and transverse stress factors ($\alpha = \sigma_h/f_{ys}$ and $\beta = \sigma_a/f_{ys}$, respectively) at the point where biaxial stresses intersect the von Mises failure envelope. Axial and transverse stress concentration factors (α and β, respectively) for CFST columns are presented in Table 3. Figure 6a compares biaxial stresses obtained from NC-filled columns of different shapes. In most cases, α was greater and β was smaller for circular columns. This indicates greater transverse stresses developing in circular columns. Figure 6b compares biaxial stresses for tube columns infilled with different concretes. In most cases, LWC-filled columns had particularly higher α values and lower β values.

Concrete confinement

Axial stresses in the concrete core of filled tube columns (f_c) are determined by Eq. (2):

$$f_c = \frac{P_c}{A_c} = \frac{P - P_s}{A_c} = \frac{P - A_s\sigma_a}{A_c}, \tag{2}$$

where P is the nominal load applied across the entire columns, P_c is the load applied on the concrete core, P_s is the load applied on the steel, A_c is the concrete area, A_s is the steel tube area and σ_a is the axial stress in steel. Figure 7 shows the axial stress development in the concrete core of filled tube columns under compressive loading. Concrete axial stresses in columns NcI-3 and NcI-9 are compared in Fig. 7a to show an example of the effects of slenderness. NcI-9 had higher slenderness compared with NcI-3, and

Table 3 Axial strain and biaxial stress factors

Column designation		*L/D*	Axial strain		α	β
NcI-3	NcI-9	3–9	0.0061	0.0040	0.18–0.26	0.88–0.82
EcI-3	EcI-9	3–9	0.0108	0.0032	0.20–0.14	0.88–0.91
LcI-3	LcI-9	3–9	0.0143	0.0090	0.23–0.23	0.86–0.85
UcI-3	UcI-9	3–9	0.0045	0.0102	0.17–0.23	0.89–0.85
ScI-3	ScI-9	3–9	0.0034	0.0035	0.26–0.19	0.84–0.87
RcI-3	RcI-9	3–9	0.0037	0.0032	0.15–0.12	0.88–0.93
Nr-6	Nr-20	6–20	0.0034	0.0026	0.11–0.05	0.94–0.98
Er-6	Er-20	6–20	0.0050	0.0037	0.17–0.07	0.96–0.96
Lr-6	Lr-20	6–20	0.0066	0.0023	0.25–0.20	0.85–0.88
Ur-6	Ur-20	6–20	0.0043	0.0039	0.07–0.13	0.96–0.93
Sr-6	Sr-20	6–20	0.0045	0.0034	0.15–0.23	0.92–0.86
Rr-6	Rr-20	6–20	0.0056	0.0022	0.12–0.10	0.93–0.94
Ns4-3	Ns4-10	3–10	0.0037	0.0031	0.23–0.18	0.87–0.90
Es4-3	Es4-10	3–10	0.0125	0.0031	0.11–0.06	0.94–0.97
Ls4-3	Ls4-10	3–10	0.0061	0.0032	0.10–0.20	0.94–0.89
Us4-3	Us4-10	3–10	0.0070	0.0043	0.07–0.13	0.96–0.93
Ss4-3	Ss4-10	3–10	0.0054	0.0021	0.19–0.06	0.89–0.96
Ns2-6	Ns2-20	6–20	0.0018	0.0026	0.20–0.17	0.88–0.91
Es2-6	Es2-20	6–20	0.0026	0.0021	0.17–0.17	0.90–0.91
Ls2-6	Ls2-20	6–20	0.0036	0.0020	0.22–0.13	0.87–0.93
Us2-6	Us2-20	6–20	0.0028	0.0071	0.21–0.20	0.88–0.89
Ss2-6	Ss2-20	6–20	0.0032	0.0029	0.12–0.05	0.93–0.97
Rs2-6	Rs2-16	6–16	0.0023	0.0020	0.10–0.14	0.95–0.92

axial stress decreased at a higher rate after a maximum was reached. Figure 7a also compares concrete axial stress of NC-filled steel tubes with different shapes. Steel tubes with greater thickness ('cI' had the highest thickness, followed by 's4', 'r' and 's2') were capable of maintaining comparatively greater stress as strain increases.

Figure 7b compares the axial concrete stress development in CFSTs with different infill. Columns ScI-3, UcI-3 and NcI-3 (infilled with SCC, UHSC and NC, respectively) shared similar concrete axial stress behaviour at early stages of loading. The UHSC-filled column maintained comparably less stress after a maximum value was reached. RcI-3 and LcI-3 infilled with CRC and LWC shared similar concrete axial stress development at early stages of loading. However, the LWC-filled column was able to take higher stress than its CRC-filled counterpart. The ECC-filled column (EcI-3) developed increased stress at a slightly higher rate compared with both RcI-3 and LcI-3. At axial strain of about 0.005, EcI-3 and LcI-3 began to conform to very similar stress behaviour.

The concrete axial stress–strain behaviour of CFSTs shown in Fig. 7 is used to determine experimental concrete confined strength (f'_{cc}). The concrete axial stress at ultimate axial load of each CFST is f'_{cc}. Experimental concrete confined strength for each CFST tested in this research is listed in Table 4. Cylinder compressive strength at the age of testing (f'_c) is also provided in Table 4, and compared with f'_{cc} by f'_{cc}/f'_c ratios. In most cases, columns with higher slenderness had lower f'_{cc}/f'_c compared with their shorter counterparts. This might be due to global instability causing columns with higher slenderness to fail before confinement fully develops. Confined concrete strength was the highest for 'cI' columns, followed by 'r', 's4' and 's2'. It should be noted that the steel tube of 'cI' columns had the largest thickness and 's2' columns had the smallest thickness compared with other shapes. Concrete confined strength decreased with the decrease in tube thickness.

However, f'_{cc}/f'_c describes how concrete strength is improved due to confinement from the presence of the steel tube. In most cases, f'_{cc}/f'_c was greater than 1, indicating that strength of confined concrete is usually greater than cylinder compressive strength. However, some columns failed before concrete confinement could fully develop, resulting in f'_{cc}/f'_c less than 1. LWC-filled columns showed the greatest strength enhancement due to confinement, with f'_{cc}/f'_c up to 2.18. NC-, CRC- and SCC-filled columns also showed significant increase in strength due to confinement, with f'_{cc}/f'_c up to 1.64, 1.66 and 1.67, respectively. On the other hand, UcI-3 yielded the lowest f'_{cc}/f'_c of 1.09 compared with other 'cI' columns. In general, weaker concretes had greater strength increase due to confinement from the steel tube. However, increasing steel geometric (for example tube

Fig. 6 Biaxial stress development in CFST columns

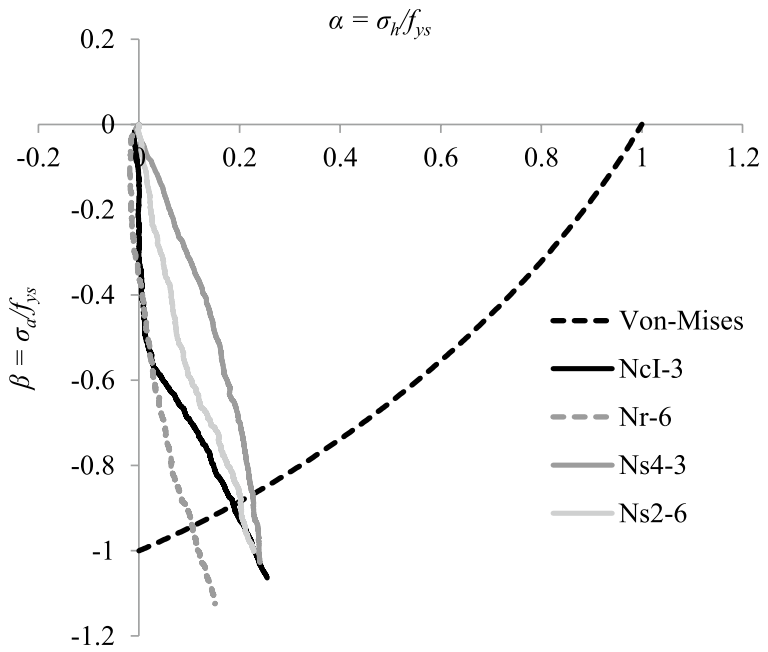

(a) Comparison of biaxial stress development in CFSTs with different shapes

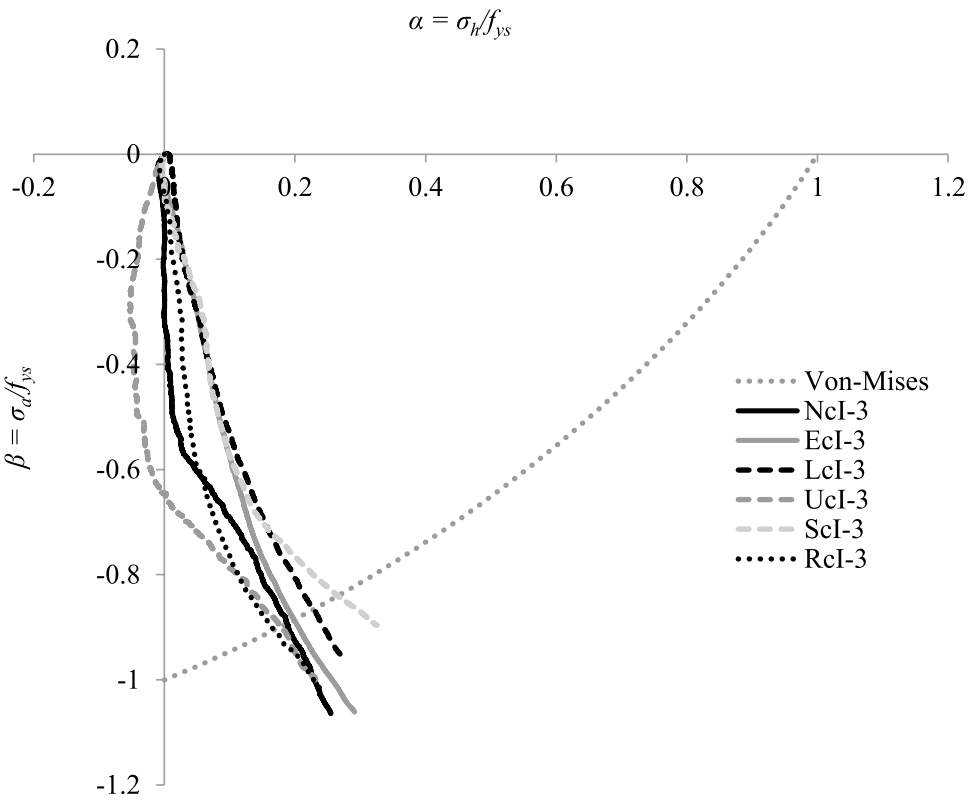

(b) Comparison of biaxial stress development in CFSTs with different in-fill

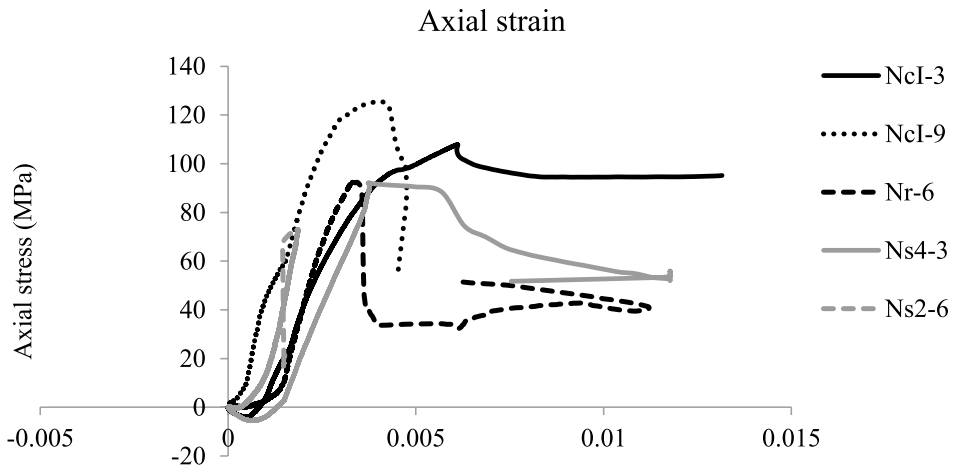

(a) Comparison of axial concrete stresses in CFST with different shapes and slenderness

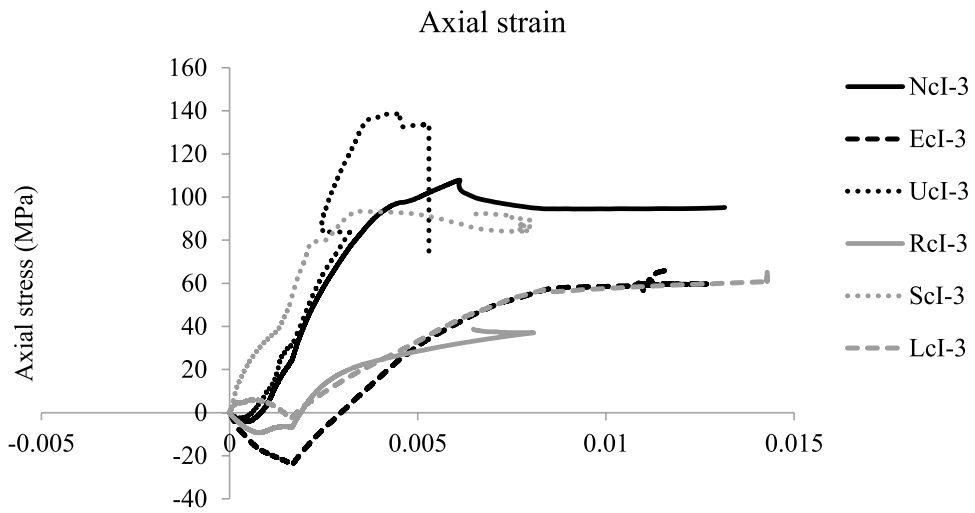

(b) Comparison of axial concrete stresses in CFST with different in-fill

Fig. 7 Axial concrete stresses during loading

thickness) and material properties may result in improved confinement of UHSC.

Analytical models for concrete confined strength

Existing models for determining concrete confined strength

Analytical models for determining concrete confined strength (f'_{cc}) had been developed by Richart et al. (1928), Mander et al. (1988) and O'Shea and Bridge (2000) and modified by Lachemi et al. (2006). The Richart et al. (1928) model for concrete confined strength was developed based on experimentation of concrete specimens under triaxial compression from hydraulic pressure. The Mander et al. (1988) model was developed to determine strength of concrete confined by bar reinforcements. O'Shea and Bridge (2000) then modified the Mander et al. (1988) concrete confinement model to make it applicable for CFST columns. The three concrete confinement models are provided in Eqs. (3) to (5) with subscripts 'R', 'M' and 'O' representing models from Richart et al. (1928), Mander et al. (1988) and O'Shea and Bridge (2000), respectively:

$$f'_{cc(R)} = f'_c + k_1 \frac{2t\alpha f_{ys}}{D-2t} = f'_c + 4.1\frac{2t\alpha f_{ys}}{D-2t} \tag{3}$$

$$f'_{cc(M)} = f'_c\left(2.254\sqrt{1+15.88\frac{t\alpha f_{ys}}{f'_c(D-2t)}} - 4\frac{t\alpha f_{ys}}{f'_c(D-2t)} - 1.254\right) \tag{4}$$

Table 4 Concrete confined strength and strength enhancement

Column		f'_c, MPa	f'_{cc}, MPa		f'_{cc}/f'_c	
NcI-3	NcI-9	66	108	126	1.64	1.91
EcI-3	EcI-9	50	60	68	1.21	1.37
LcI-3	LcI-9	36	79	57	2.18	1.59
UcI-3	UcI-9	127	139	125	1.09	0.99
ScI-3	ScI-9	56	93	74	1.67	1.33
RcI-3	RcI-9	46	77	62	1.66	1.34
Nr-6	Nr-20	66	92	71	1.41	1.09
Er-6	Er-20	50	35	49	0.71	0.98
Lr-6	Lr-20	36	53	44	1.47	1.21
Ur-6	Ur-20	127	113	102	0.89	0.81
Sr-6	Sr-20	56	78	79	1.40	1.41
Rr-6	Rr-20	46	47	55	1.02	1.18
Ns4-3	Ns4-10	66	92	89	1.40	1.36
Es4-3	Es4-10	50	58	51	1.17	1.02
Ls4-3	Ls4-10	36	52	47	1.45	1.30
Us4-3	Us4-10	127	124	117	0.98	0.92
Ss4-3	Ss4-10	56	69	38	1.23	0.68
Ns2-6	Ns2-20	66	73	91	1.11	1.38
Es2-6	Es2-20	50	32	35	0.65	0.71
Ls2-6	Ls2-20	36	39	34	1.07	0.94
Us2-6	Us2-20	127	102	99	0.80	0.78
Ss2-6	Ss2-20	56	42	50	0.75	0.90
Rs2-6	Rs2-16	46	26	28	0.57	0.60

$$f'_{cc(O)} = f'_c\left(2.172\sqrt{1+14.92\frac{t\alpha f_{ys}}{f'_c(D-2t)}}-4\frac{t\alpha f_{ys}}{f'_c(D-2t)}-1.228\right), \tag{5}$$

where f'_c is the concrete control cylinder compressive strength, t is the steel tube thickness, D is the outer tube diameter, α is the transverse stress factor (determined experimentally from Table 3) and f_{ys} is the yield strength of steel. Hossain (2003) also introduced a model for confined strength of concrete provided in Eq. (6), where subscript 'H' denotes the author, d is the concrete diameter and f_p is the modified unconfined compressive strength of concrete in Eq. (7):

$$f'_{cc(H)} = f_p + 4.1\frac{2t}{D-2t}\alpha f_{ys} \tag{6}$$

$$f_p = 1.61(d)^{-0.1}f'_c. \tag{7}$$

Table 5 provides concrete confined strength calculated by models from Richart et al. (1928), Mander et al. (1988), O'Shea and Bridge (2000) and Hossain (2003) in Eqs. (3) to (6), respectively. Concrete confined strength obtained experimentally is also provided in Table 5 for comparison with results from analytical models. In most cases, the four concrete confinement models tended to overestimate the strength of columns with higher slenderness. For example, the Mander et al. (1988) model predicts 58 MPa concrete confined strength for column Ls4-10, which is 25% more than the experimental value. In contrast to its shorter counterpart, the Mander et al. (1988) model predicted concrete confined strength that is 93% of the experimental value for column Ls4-3. The four models also performed better when cross-sectional area of columns was larger. For example, the concrete confined strength of ECC-filled columns predicted by the Richart et al. (1928) model predicted 98% of the experimental value for the 's4' (square) shape, 124% for 'cI' (circular), 143% for 'r' (rectangular) and 201% for 's2' (square). The results yielded by analytical model are closest to experimental concrete confined strength for the columns with the largest area and increasingly over-predicted the strength as area decreased.

In addition, the four concrete confinement models did not achieve the same performance for different types of concrete. Analytical models for concrete confinement performed best for columns infilled with NC, as overestimations remained within 125% of experimental results. Concrete confinement models yielded values up to 178% of experimental results for LWC-, UHSC- and SCC-filled columns, and up to 233% for their CRC- and ECC-filled counterparts. The Mander et al. (1988) and O'Shea and Bridge (2000) models assumed

Table 5 Experimental and theoretical confined concrete strength

Column		Confined concrete strength (f'_{cc}), MPa									
		Experimental		Richart et al. (1928)		Mander et al. (1988)		O'Shea and Bridge (2000)		Hossain (2003)	
NcI-3	NcI-9	108	126	89	96	98	107	90	98	89	97
EcI-3	EcI-9	60	68	74	68	82	75	76	69	74	68
LcI-3	LcI-9	79	57	62	62	68	68	62	62	62	62
UcI-3	UcI-9	139	125	148	156	160	170	149	158	149	156
ScI-3	ScI-9	93	74	89	79	98	88	90	81	89	80
RcI-3	RcI-9	77	62	65	62	73	68	67	63	66	62
Nr-6	Nr-20	92	71	79	72	86	75	80	70	82	74
Er-6	Er-20	35	49	72	59	80	64	73	60	74	61
Lr-6	Lr-20	53	44	68	62	73	68	67	62	69	64
Ur-6	Ur-20	113	111	147	163	159	180	148	166	152	168
Sr-6	Sr-20	78	79	75	86	83	96	77	88	78	89
Rr-6	Rr-20	47	55	62	60	69	66	64	61	64	61
Ns4-3	Ns4-10	92	89	85	81	93	89	86	82	85	81
Es4-3	Es4-10	58	51	59	55	64	58	60	54	59	55
Ls4-3	Ls4-10	52	47	45	53	49	58	45	54	45	53
Us4-3	Us4-10	127	117	138	143	145	153	136	142	138	143
Ss4-3	Ss4-10	69	38	72	61	80	65	74	60	73	62
Ns2-6	Ns2-20	73	91	83	80	92	88	85	81	88	85
Es2-6	Es2-20	32	35	65	65	72	71	66	66	69	68
Ls2-6	Ls2-20	39	34	55	47	61	52	56	48	58	50
Us2-6	Us2-20	102	99	147	141	157	150	147	140	156	151
Ss2-6	Ss2-20	42	50	67	60	72	63	67	59	71	65
Rs2-6	Rs2-16	26	28	55	59	59	65	55	60	58	62

that concrete confined strength is directly proportional to concrete unconfined compressive strength. However, experimental results showed that higher-strength concretes often undergo less confinement, and the relationship between concrete confined strength and unconfined compressive strength is not directly proportional. Therefore, the Mander et al. (1988) and O'Shea and Bridge (2000) models tended to overestimate concrete confined strength of filled tube columns to a comparatively greater degree. The Richart et al. (1928) and Hossain (2003) models often yielded similar results. However, the Richart et al. (1928) was slightly more conservative. Conservativeness is preferred as opposed to overestimation in structural design.

Proposed modification of existing concrete confinement models

The Richart et al. (1928) model predicted concrete confined strength between 80 and 110% of experimental values than the other three models. Research by Richart et al. (1928) determined the coefficient, $k_1 = 4.1$, found in Eq. (3) by testing NC samples. However, it was noted that performance of concrete confinement models was dependent on concrete type and column shape. Furthermore, existing models assume that rectangular and square columns can be converted to an equivalent circular section when calculating concrete confined strength. In order to determine the

Table 6 Confinement factors

Concrete	Concrete factor (ψ)	Shape factor (ξ)			
		Circular (c)	Rectangular (r)	Square (s4)	Square (s2)
NC	1.84	1	1.07	0.75	0.23
ECC	0.42	1	− 0.37	2.64	− 3.32
LWC	0.78	1	0.67	2.43	0.17
UHSC	0.55	1	− 2.78	− 0.38	− 2.45
CRC	0.28	1	0.22	NA	− 1.13
SCC	1.14	1	1.03	0.69	− 8.43

confinement factor associated with each type of concrete, the coefficient (k_1) was isolated for each of the shorter columns (with slenderness of 3–6). Experimental f'_{cc} and α were used to determine k_1 based on Eq. (3). Each of the k_1 values for cI-3 (circular columns with slenderness of 3) columns was divided by 4.1 to determine the concrete factor (ψ) listed in Table 6. The k_1 for each shape was divided by that of its circular counterpart to determine the shape factor (ξ) listed in Table 6.

The concrete factor (ψ) describes how confinement changes with concrete type. The shape factor (ξ) describes how confinement changes for square and rectangular sections of each concrete type. It can be noted that certain shape factors are of negative values, because the concrete confined strength was actually less than the cylinder compressive strength. This may be due to difference in failure modes, as square and rectangular columns often experienced more local buckling compared with circular ones.

Equation (3) can then be modified to account for concrete type and column shape in Eq. (8) where subscript 'P' stands for the proposed model:

$$f'_{cc(P)} = f'_c + \psi\xi 4.1\frac{2t\alpha f_{ys}}{D-2t}. \quad (8)$$

Table 7 Performance evaluation of concrete confinement models

Column	f'_{cc}, MPa		Theoretical/experimental ratio				
	Test	Proposed model (Eq. 8)	Proposed model (Eq. 8)	Hossain (2003)	Richart et al. (1928)	Mander et al. (1988)	O'Shea and Bridge (2000)
NcI-9	126	122	0.97	0.83	0.82	0.91	0.84
EcI-9	53	57	1.07	1.24	1.24	1.37	1.26
LcI-9	57	86	1.50	1.11	1.10	1.20	1.10
UcI-9	125	143	1.14	1.08	1.07	1.15	1.07
ScI-9	74	83	1.11	1.28	1.27	1.41	1.30
RcI-9	47	51	1.07	0.96	0.95	1.05	0.96
Nr-20	71	77	1.08	0.89	0.86	0.93	0.87
Er-20	49	48	0.99	1.60	1.55	1.72	1.58
Lr-20	44	50	1.14	1.32	1.29	1.38	1.26
Ur-20	102	101	0.99	1.26	1.21	1.26	1.18
Sr-20	79	92	1.16	1.36	1.32	1.46	1.35
Rr-20	55	47	0.86	0.99	0.96	1.06	0.98
Ns4-10	89	87	0.97	0.93	0.92	1.01	0.94
Es4-10	51	56	1.09	0.99	0.98	1.07	0.99
Ls4-10	47	67	1.44	0.86	0.85	0.93	0.86
Us4-10	117	123	1.06	1.12	1.11	1.16	1.09
Ss4-10	38	60	1.58	1.06	1.05	1.16	1.07
Ns2-20	91	72	0.79	1.21	1.14	1.25	1.16
Es2-20	35	29	0.82	2.41	2.27	2.51	2.32
Ls2-20	34	38	1.11	1.50	1.43	1.59	1.46
Us2-20	99	103	1.04	1.53	1.43	1.53	1.43
Ss2-20	50	50	1.00	2.23	2.09	2.26	2.11
Rs2-16	28	17	0.61	1.69	1.58	1.72	1.59
Lachemi et al. (2006b)							
CI-SCC-4.8a;b	90	81	0.90	0.87	0.86	0.96	0.88
CI-SCC-4.8a;b	80	81	1.01	0.98	0.97	1.08	0.99
CI-NC-4.8a;b	96	98	1.02	0.80	0.80	0.89	0.82
CI-NC-4.8a;b	81	98	1.20	0.95	0.95	1.05	0.97
CI-SCC-9.5a;b	83	79	0.95	0.92	0.91	1.01	0.93
CI-SCC-9.5a;b	72	79	1.09	1.06	1.05	1.17	1.07
CI-NC-9.5a;b	101	80	0.80	0.67	0.67	0.74	0.68
CI-NC-9.5a;b	80	80	1.01	0.85	0.84	0.93	0.86
		Mean ratio	1.05	1.18	1.15	1.26	1.16

Since the concrete and shape factors in Table 6 were determined based on short columns (slender ratio from 3 to 6) tested in this research, the more slender columns (slenderness ratio from 9 to 20) were used to evaluate the performance of the proposed model in Eq. (8). In addition, external data from experimental results of Lachemi et al. (2006) were also taken for performance evaluation of concrete confinement models in Table 7. Concrete confined strength determined by Eq. (8) is listed in Table 7, along with theoretical/experimental ratios for each model.

The Richart et al. (1928) model yielded theoretical/experimental ratios between 0.80 and 1.10 for 42% of columns, and the maximum over-prediction was up to 2.27 times the experimental value. The Mander et al. (1988) model yielded theoretical/experimental ratios between 0.80 and 1.10 for 32% of columns, and the maximum over-prediction was up to 2.51 times the experimental value. The O'Shea and Bridge (2000) and Hossain (2003) models both yielded theoretical/experimental ratios between 0.80 and 1.10 for 39% of columns, and the maximum over-prediction was up to 2.32 and 2.41 times the experimental value, respectively.

The proposed model (Eq. 8) yielded theoretical/experimental ratios between 0.80 and 1.10 for 61% of columns, and the maximum over-prediction was up to 1.58 times the experimental value. This is also evident from the mean theoretical-to-experimental ratio of 1.05 for the proposed model. The proposed model shows improvement in estimating the concrete confined strength of CFST columns.

Conclusions

Forty-six concrete-filled steel tube (CFST) columns were tested under concentric axial compression. Six concretes were used as infill for steel tube columns including normal concrete (NC), ultrahigh-strength concrete (UHSC), engineered cementitious composite (ECC), lightweight concrete (LWC), ordinary self-consolidating concrete (SCC) and crumb rubber concrete (CRC). Columns also ranged in slenderness and shape, including circular, square and rectangular sections. Load–displacement response, failure modes, strain characteristics and concrete confined strength of columns were compared. Performance of existing concrete confinement models was evaluated, and a modified model is proposed to accommodate different concrete types, column shapes and slenderness. Main conclusions of this research are as follows:

- Column slenderness and shape as well as concrete type/strength had an effect on CFST column failure modes. Five failure modes such as radial expansion, local buckling, plastic hinge formation (at region of successive close local buckles causing bending and subsequent regional yielding), shear (at a local buckle) and global buckling were identified. Columns with lower slenderness ratio failed by radial expansion. As slenderness increased to 6, columns failed by local buckling or shear. Columns slenderness from 9 to 20 failed by global buckling or shear. Square columns failed more often by local buckling. Columns with higher-strength concrete failed by shear more often than those with low concrete strength.
- Column slenderness and concrete strength also had an effect on axial load–displacement response. More slender columns failed soon after the first peak load was reached, while short columns continued to take load. Columns with higher-strength concretes showed higher distinctive peak load. Columns with comparatively lower-strength concretes transitioned from elastic to plastic stages without a significant peak load. In general, an increase in axial strength with the increase in slenderness of columns was observed with exceptions of few columns.
- Axial and transverse strain behaviour of CFSTs depended on cross-sectional shape/area, concrete type and slenderness. CFST columns with comparatively lower-strength concretes (such as ECC, LWC and CRC) developed higher axial and transverse strain in steel tube compared to those with NC, UHSC and SCC. CFST with LWC having the lowest compressive strength experienced the highest axial strain of 0.0143. Axial and transverse strains in steel tube exceeded yield strain before ultimate capacity of columns in most cases.
- Biaxial stress factors were mainly dependent on cross-sectional shape, since circular columns had higher transverse stress factor compared with square and rectangular ones. On the other hand, square and rectangular columns had higher axial stress factors. This indicates greater transverse stress development in circular CFST columns providing more confining effect.
- Concrete confined strength was dependent on concrete type, column slenderness/shape and steel thickness. Columns with greater tube thickness had higher confined concrete strength. More slender columns typically had lower concrete confined strength. The strength enhancement due to concrete confinement from the steel tube decreases with increasing concrete compressive strength. Weaker concretes had produced higher confining strength increase due to tube confinement. LWC showed 2.18 times higher confined concrete strength than unconfined concrete strength compared to 1.09 times of UHSC.
- Existing analytical models for estimating confined strength of concrete performed best for those CFST columns infilled with NC (within 125% of experimental values). Performance decreased for columns infilled with LWC, UHSC, SCC, CRC and ECC. Concrete confinement models which assumed direct proportionality

between concrete confined strength and cylinder compressive strength did not perform as well (up to 233% of experimental value).

- Concrete and shape factors were proposed to improve existing concrete confinement models. Predicted concrete confined strength using the proposed model was improved as theoretical values were generally close to experimental ones (with a mean theoretical-to-experimental ratio of 1.05).

Acknowledgements Authors acknowledge the financial support from National Science and Engineering Research Council (NSERC) of Canada for this project.

References

Fam A, Qie FS, Rizkalla S (2004) Concrete filled steel tubes subjected to axial compression and lateral cyclic loads. J Struct Eng 130(4):631–640

Ghosh RS (1977) Strengthening of slender hollow steel columns by filling with concrete. Can J Civ Eng 4(2):127–133

Han LH, Zhao XL, Tao Z (2003) Concrete-filled thin-walled steel SHS and RHS beam-columns subjected to cyclic loading. Thin Wall Struct 41(9):801–833

Han LH, Yao GH, Zhao XL (2005) Tests and calculations of hollow structural steel (HSS) stub columns filled with self-consolidating concrete (SCC). J Constr Steel Res 61(9):1241–1269

Hassan AAA, Lachemi M, Hossain KMA (2012) Effect of metakaolin and silica fume on rheology of self-consolidating concrete. ACI Mater J 109(6):657–664

Hossain KMA (2003) Behaviour of thin walled composite columns under axial loading. Compos Part B Eng 34(8):715–725

Hossain KMA (2004) Properties of volcanic pumice based cement and lightweight concrete. Cement Concrete Res 34(2):283–291

Hossain KMA, Mak C, Ametrano D (2012a) GFRP reinforced UHPC composites for sustainable bridge construction. Can Civ Eng 29(1):12–15

Hossain KMA, Lachemi M, Sammour M, Sonebi M (2012b) Influence of polyvinyl alcohol, steel and hybrid fibers on fresh properties of self-consolidating concrete. Constr Build Mater 31(6):320–325

Hossain KMA, Ametrano D, Lachemi M (2018) The bond between GFRP Bars and ultra-high strength concrete. Constr Mater J 171(4):161–176

Khaloo A, Raisi EM, Hosseini P, Tahsin H (2014) Mechanical performance of self-compacting concrete reinforced with steel fibers. Constr Build Mater 51(1):179–186

Lachemi M, Hossain KM, Lambros V (2006a) Axial load behavior of self-consolidating concrete filled steel tube columns in construction and service stages. ACI Struct J 103(1):38–47

Lachemi M, Hossain KM, Lambros V (2006b) Self-consolidating concrete filled steel tube columns—design equations for confinement and axial strength. Struct Eng Mech 22(5):541–562

Lotfy A, Hossain KMA, Lachemi M (2016) Durability properties of lightweight self-consolidating concrete with three aggregates. Constr Build Mater 113(5):679–700

Mander JB, Priestly MJN, Park R (1988) Theoretical stress-strain model for confined concrete. J Struct Eng 114(8):1804–1826

Mohammed BS, Hossain KMA, Swee JTE, Wong G, Abdullahi M (2012) Properties of crumb rubber hollow concrete block. J Clean Prod 23(1):57–67

O'Shea MD, Bridge RQ (2000) Design of circular thin-walled concrete filled steel tubes. J Struct Eng 126(11):1295–1303

Özbay E, Karahan O, Lachemi M, Hossain KMA, Atis CD (2013) Dual effectiveness of freezing–thawing and sulfate attack on high-volume slag-incorporated ECC. Comp Part B-Engng 45(1):1384–1390

Richart FE, Brandtzaeg A, Brown RL (1928) A study of the failure of concrete under combined compressive stresses. Bulleting #185, University of Illinois, Engineering Experimental station, Urbana, Ill

Shanmugam NE, Lakshmi B (2001) State of the art report on steel–concrete composite columns. J Constr Steel Res 57(10):1041–1080

Sherir MAA, Hossain KMA, Lachemi M (2018) Permeation and transport properties of self-healed cementitious composite produced with MgO expansive agent. ASCE J Mater Civ Eng 30(11):01018291

Weimann MB, Li VC (2003) Drying shrinkage and crack width of ECC. In: Proceedings of the 7th international conference: Brittle Matrix Composites. Warsaw, 13–15 October, 2003, pp 37–46

Yu Q, Tao Z, Wu Y (2008) Experimental behaviour of high performance concrete filled steel tubular columns. Thin Wall Struct 46(4):362–370